Research Square

Preprints are preliminary reports that have not undergone peer review.
They should not be considered conclusive, used to inform clinical practice,
or referenced by the media as validated information.

# Integrating Vernier Spectrum With Fano Resonance for High Sensitivity of All-optical Sensor

**Mohammad Amirul Hairol Aman**
Universiti Islam Antarabangsa Malaysia: International Islamic University Malaysia
**Ahmad Fakhrurrazi Ahmad Noorden** ( fakhrurrazi@iium.edu.my )
International Islamic University Malaysia https://orcid.org/0000-0002-4356-9059
**Faris Azim Ahmad Fajri**
Universiti Islam Antarabangsa Malaysia: International Islamic University Malaysia
**Muhammad Zamzuri Abdul Kadir**
Universiti Islam Antarabangsa Malaysia: International Islamic University Malaysia
**Iskandar Bahari**
Universiti Islam Antarabangsa Malaysia: International Islamic University Malaysia
**Wan Hazman Danial**
Universiti Islam Antarabangsa Malaysia: International Islamic University Malaysia
**Suzairi Daud**
Universiti Teknologi Malaysia - Main Campus Skudai: Universiti Teknologi Malaysia
**Mahdi Bahadoran**
Shiraz University of Technology

**Research Article**

**Keywords:** Fano Resonance, Vernier effect, Microring, Coupling Coefficient, Sensitivity

**Posted Date:** June 22nd, 2022

**DOI:** https://doi.org/10.21203/rs.3.rs-1349288/v1

**License:** This work is licensed under a Creative Commons Attribution 4.0 International License.
Read Full License

# INTEGRATING VERNIER SPECTRUM WITH FANO RESONANCE FOR HIGH SENSITIVITY OF ALL-OPTICAL SENSOR

Mohammad Amirul Hairol Aman[1], Ahmad Fakhrurrazi Ahmad Noorden[1*], Faris Azim Ahmad Fajri[1], Muhammad Zamzuri Abdul Kadir[1], Iskandar Bahari[1], Wan Hazman Danial[2], Suzairi Daud[3], Mahdi Bahadoran[4]

[1] Centre for Advanced Optoelectronics Research (CAPTOR), Kulliyyah of Science, International Islamic University Malaysia, 25200 Kuantan, Pahang, Malaysia
[2] Department of Chemistry, Kulliyyah of Science, International Islamic University Malaysia, 25200 Kuantan, Pahang, Malaysia
[3] Laser Center, Ibnu Sina Institute for Scientific & Industrial Research, Universiti Teknologi Malaysia, 81310 Johor Bahru, Johor.
[4] Department of Physics, Shiraz University of Technology, 31371555, Shiraz, Fars, Iran

* Ahmad Fakhrurrazi Ahmad Noorden, E-mail: fakhrurrazi@iium.edu.my

**KEYWORDS:** Fano Resonance, Vernier effect, Microring, Coupling Coefficient, Sensitivity

**ABSTRACT:**

Vernier and Fano resonances are promising approaches for enhancing the sensitivity of an all-optical sensor. A theoretical analysis was performed to integrate a Fano-like resonance shape with a Vernier resonance by considering the presence of partial reflective end facets at a double microring resonator waveguide. The system was developed based on scattering matrix and optical transfer function. The double and all-pass racetrack microring configurations were compared with and without the end facet at the waveguide to analyze the dynamic change of the output resonance spectrum. The spectrum were analyzed based on the free spectral range and resonance pattern. The resonator systems were applied to refractive index-based sensing protocol, which was operated by a shift of resonance wavelength with a change of refractive index. The sensitivity was optimized by varying the configuration parameters such as the radius of the ring, the distance between end facet, and the coupling coefficients. Integrating Vernier spectrum with Fano resonance improved the sensitivity for all-pass racetrack configuration by 5.16 % and the sensitivity for double racetrack configuration by 6.31 %. The recorded limit of detection (LOD) of double racetrack was $3.30 \times 10^{-5}$.

## 1.0 INTRODUCTION

All-optical sensing has become a promising technique in developing a sensor device. The sensing technology operates based on the direct interaction between the sensing environment and an evanescent wave of propagated light [1, 2]. This approach has been found to be more stable with the presence of electromagnetic disturbance compared to electrical-based sensors [3]. Thus, it has been applied to various fields of sensing such as gas [4], biosensing [5–7], chemical [8], temperature [9, 10] and pressure sensor [11]. Having high sensitivity is the most crucial property in all-optical sensing technology, which can be achieved by optimizing the geometrical configuration [12], and material properties [13], as well as employing Fano resonance [14, 15] and Vernier effect [10, 16–18].

Fano resonance can be obtained by using an interferometric type resonator. Fano resonance has an asymmetrical line-shape where the wavelength shift can be increased significantly, thus improving the sensing capabilities of the device [16]. Fano resonance has been used in sensing fields such as high-temperature sensors [13, 14], high-accuracy vibration sensors [13, 14], and acoustic wave sensors [13, 15]. Practically, the reflector can be fabricated by micro-drilling the waveguide as performed by [19], where two air-holes were designed as the reflectors. Multiple sharp peaks of Fano resonance have been found by analyzing the interference between subradiant modes and the magnetic dipole resonance mode. This method produces 370 nm/RIU sensitivity with $10^5$ Q factor magnitude. The Fano resonance-based sensor was performed by introducing a destructive interaction between surface plasmon polariton and local surface plasmon in stub-shaped defect of the metasurface. The maximum sensitivity achieved is 535 nm/RIU, which is claimed to be three times higher than the conventional surface plasmon resonance system [20]. However, Fano resonance has a low Free Spectral Range (FSR) [16]. Low FSR leads to small limit of detection (LOD). The LOD is an important aspect that needs to be considered because it is the measurement of the smallest possible value a sensor can evaluate [21].

Optical Vernier effect is also an alternative solution for enhancing the sensitivity of all-optical devices [22, 23]. The effect occurs as two resonance lights interact in a medium and produce a superimposed spectrum [24]. The spectrum is produced in the form of an envelope-like shape and can enhance the magnitude of the wavelength shift. This allows the all-optical sensing signal to reach better resolution of measurements. There are several types of resonator mediums which are used for utilizing Vernier effect in sensing operation such as microfiber knot [18], interferometric resonator [17], and microresonator [25]. For microresonators, the Vernier effect-based sensor was performed by a hybrid structure of two polymer-cascaded

configurations, in which one of them consists of a Mach-Zehnder system [22]. The sensitivity of Vernier effect-based microresonator achieves up to 578 nm/RIU by using 3×3 linearly distributed optical coupler [5]. However, the conventional Vernier effect sensing spectrum may not reach a high detection performance.

In this work, both concepts of Fano resonance and Vernier effect was utiized for optimizing the FSR and sensitivity of the microresonator system. Two configurations, double and all-pass racetrack were used for the resonance medium where the reflectors generate Fano resonance spectrum. The two configurations were compared and analyzed, focusing on the Fano resonance and the Vernier effect. The investigation was based on asymmetrical resonance properties, the LOD, and the sensitivity for geometrically optimized microring system. The LOD was analyzed through the distance of FSR, and the sensitivity was obtained through wavelength shift with various refractive indexes.

## 2.0 MODEL & THEORY

The Fano resonance can be obtained by using a microring resonator waveguide coupled with Mach-Zehnder interferometers [26], and a microring resonator with feedback coupled waveguide [14]. In this research, the Fano resonance was analyzed based on the two configurations of microring resonator with end-facet reflection at the bus waveguide as shown in Fig. 1. The light goes through the input port, $E_{in}$, and splits to two paths at the coupling region. One portion of the light is coupled inside the ring waveguide, $iS_1$, and the other portion travels in the bus waveguide, $C_1$ [27]. Inside the bus waveguide, the light exhibits a resonance phase shift, which happen because the light bounces back and forth between the two partial reflective end facets. The light intensity builds-up due to the resonance effect as it travels within the circulation path of the ring waveguide. The resonance light inside the microring waveguide experiences an optical phase shift [28] as $\xi$ and $\xi_{1,2}$ for all-pass racetrack and double racetrack configuration, respectively. Constructive interference occurs as the resonance light is in phase with the incoming light in the bus waveguide. Thus, the resonance spectrum is obtained at the output port of the waveguide. The spectrum is different based on the configuration parameters such as the radius of ring, length of waveguide, phase difference, and coupling coefficients. Both configurations were simulated based on silicon-on-insulator (SOI) material, which consists of Si core and $SiO_2$ substrate as shown in Fig. 1.

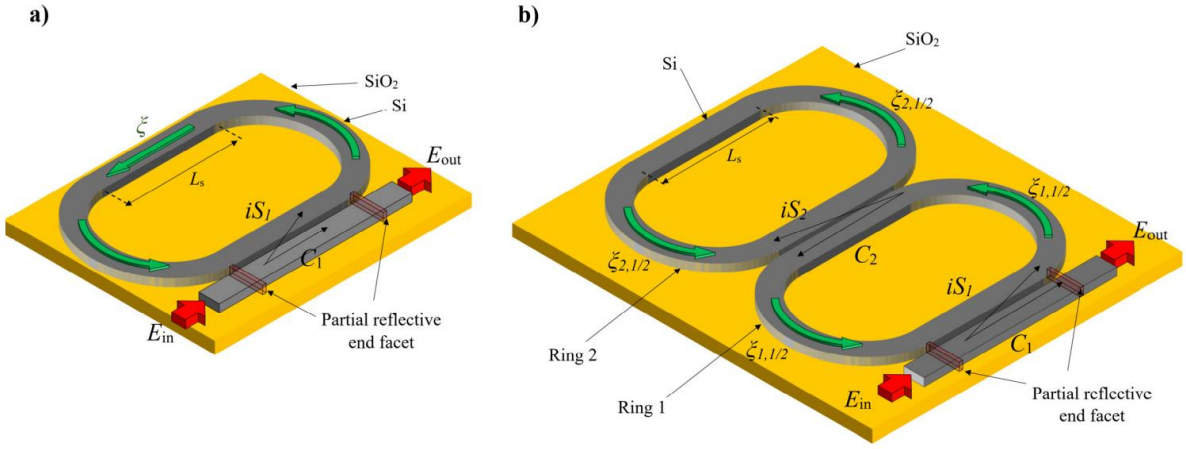


**Fig. 1** a) All-pass racetrack microring and b) double racetrack microring with end-facet reflection. Light goes through the input port, $E_{in}$ and through the ring. The light is transmitted through the output port, $E_{out}$

The transfer matrix of total resonance for both configurations is correlated with end- facet reflection as [19]

$$\begin{bmatrix} E_{out} \\ E_1 \end{bmatrix} = \mathrm{M}_h \mathrm{M}_1 \mathrm{M}_R \mathrm{M}_1 \mathrm{M}_h \begin{bmatrix} E_{in} \\ E_2 \end{bmatrix}, \tag{1}$$

where $\mathrm{M_h}$ is the partially reflecting end facet [29] which is determined by

$$\mathrm{M}_h = \frac{1}{i\sqrt{1-r_h^2}} \begin{bmatrix} -1 & -r_h \\ r_h & 1 \end{bmatrix}. \tag{2}$$

The amplitude reflection coefficient, $\mathrm{r_h}$ [19], is computed based on the ratio of effective refractive index, $\mathrm{n_{eff}}$ as

$$r_h = \frac{n_{eff} - 1}{1 - n_{eff}} \text{ [29]}. \tag{3}$$

The effective refractive index is calculated based on the Marcatilli's approach. Unlike [30, 31] that modelled the refractive index for non-linear material, the simpler method was used in this study, which is finding the effective index based on the cross-sectional waveguide for linear materials such in [28, 32]. There are three materials within the cross-section which are the core (Si), the substrate ($SiO_2$), and the cladding, air. The transfer matrix, $\mathrm{M_1}$ represents the light travelling through the waveguide and was used to determine the phase shift of the light. The phase shift contributes to the intensity of the interference as

$$M_1 = \begin{bmatrix} exp(-i2\pi nl/\lambda) & 0 \\ 0 & exp(-i2\pi nl/\lambda) \end{bmatrix}$$ [19]. (4)

Considering the resonance from microring waveguide, the optical transfer function is included in the total resonance as shown in Equation (1) through the resonator matrix, $M_R$. The matrix is used for both all-pass racetrack and double racetrack configurations. The resonator matrix $M_R$ is defined as

$$M_R = \begin{bmatrix} t_R & 0 \\ 0 & 1 \end{bmatrix}$$ [19], (5)

where $t_R$ is the optical transfer function of all-pass microring and double racetrack microring. Table 1 shows the configuration parameters involved and their optical transfer function equations. The single-pass amplitude $a = \exp(-\alpha L_R/2)$ and $\exp(iknL_R)$ represents the optical phase shift of all-pass racetrack microring resonator where $L_R$ is the optical path length of the system [28, 33]. For double racetrack configuration, the optical phase shift is defined as $\xi_{1,2} = \exp(-\alpha L_{1,2}/2)\exp(iknL_{1,2})$ where the $L_1$ and $L_2$ is the optical path length of ring 1 and ring 2 waveguide, respectively. The propagation loss (α) of the light that travels within the microring waveguide is considered as the dispersion parameter of the phase shift.

Table 1. Parameters and optical transfer function of All-Pass Microring Resonator and Double Racetrack Microring Resonator

| Configuration | All-Pass Microring Resonator | Double Racetrack Microring Resonator | |
|---|---|---|---|
| | | Racetrack 1 | Racetrack 2 |
| Simulated Wavelength Range, $\lambda$ | 1.4 $\mu$m - 1.7 $\mu$m [19] | 1.4 $\mu$m - 1.7 $\mu$m [19] | 1.4 $\mu$m - 1.7 $\mu$m [19] |
| Optical Transfer Function (OTF) | $\frac{E_{out}}{E_{in}} = \frac{t - ae^{i2\pi nL_R/\lambda}}{1 - tae^{i2\pi nL_R/\lambda}}$ [32] (6) | $\frac{E_{out}}{E_{in}} = \frac{c_1 - c_1^2c_2\xi_1 - c_2s_1^2\xi_2 - c_1c_2\xi_2 + c_1^2\xi_1\xi_2s_2^2 + s_1^2s_2^2\xi_1\xi_2 + c_1^2c_2^2\xi_1\xi_2 + c_2^2s_1^2\xi_1\xi_2}{1 - c_1c_2\xi_1 - c_2\xi_2 + c_1\xi_1\xi_2s_2^2 + c_1c_2^2\xi_1\xi_2}$ [28] (7) | |

In Equation (6) and (7), there are self-coupling coefficient, $t, c_{1,2} = \sqrt{1-\kappa_{1,2}}\sqrt{1-\gamma_{1,2}}$ [25] and cross-coupling coefficient, $s_{1,2} = \sqrt{\kappa_{1,2}}\sqrt{1-\gamma_{1,2}}$ [28], where $\kappa$ is coupling coefficient [28] and $\gamma$ is loss coefficient [28]. The normalized intensity was computed by squaring the

optical transfer function and plotting it against the wavelength domain. All-pass racetrack configuration was used to compare the WGM resonance spectrum with WGM plus Fano resonance. The double racetrack configuration was applied to integrate the Fano resonance and Vernier resonance.

### 3.0 VERNIER AND FANO RESONANCE SPECTRUM

The total resonance transfer matrix for both configurations was used to simulate the output resonance spectrum in the wavelength range of 1.4 to 1.7 µm. The spectrum in Fig. 2 was validated by comparing it with the literature [19]. The finding is in good agreement with each other. In the spectrum, there are several noticeable Fano-like line-shape, and asymmetrical resonances as shown in Fig. 2 at the 1.538 to 1.540 µm double peak [28]. Special features of Fano resonance is the sharp dip [34] with local maximum and minimum as shown in Fig. 2. The occurrence of Fano resonance due to interference between two states which are discrete and continuum state [35].

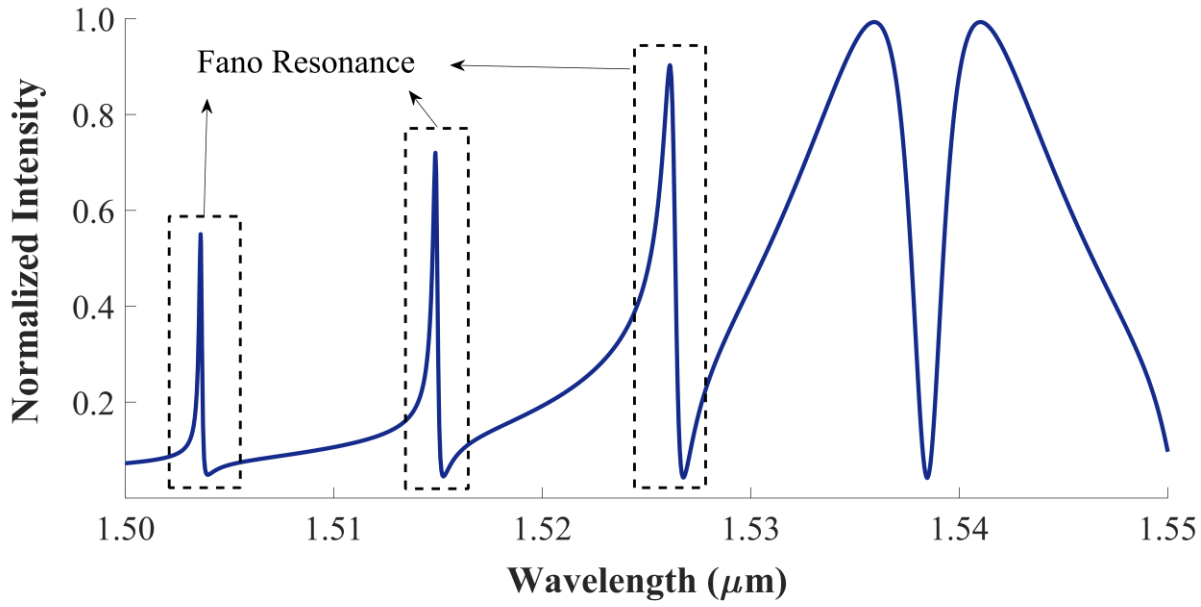


**Fig. 2** Simulated Fano resonance spectrum for all-pass configuration. The dashed boxes are Fano resonance

The simulation for all-pass racetrack microring with end-facet was performed by varying the microring, radius (R) ranging from 2.00 µm to 20.00 µm and the end facet length of waveguide ($L_S$) from 5.00 to 15.00 µm. Fig. 3 a) shows the output spectrum for the all-pass racetrack

microring system. As for the double racetrack with end-facet system, coupling coefficient 1, ($\kappa_1$) and coupling coefficient 2, ($\kappa_2$) were set as constant with value 0.95. The varied parameters of this simulation are the radii of ring 1, ($R_1$) and ring 2, ($R_2$) which were set from 2.00 to 20.00 µm and the distance between end-facet from 5.00 to 15.00 µm. Fig. 3 b) shows the output spectrum for the double racetrack microring resonator. The spectrum shows a wave packet pattern which represents the combination of resonance effects in two different microring waveguides. Both spectrums exhibit an asymmetrical resonance Fano-like shape. These shapes as shown Figs. 3 a) and b) are different compared to the conventional microring and their occurrences are the contributions of the extra features in the microring which is the end-facet reflection.

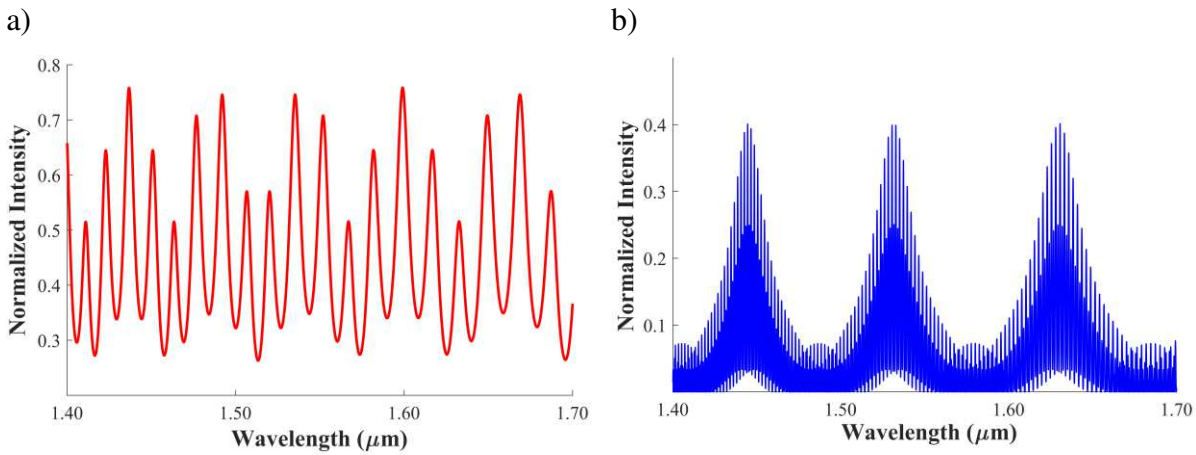


**Fig. 3** Spectrum of a) all-pass microring resonator and b) double racetrack microring resonator with end-facet

Fano resonance is initiated through the partially reflecting wave in the waveguide by end-facet reflection on both sides of the bus waveguide. It is generated due to the resonance in the microring waveguide that forms a WGM and merges with the Fano resonance in the bus waveguide. Due to its profile of having sharp peak, Fano resonance can be utilized in various applications such as sensors, modulators, and lasers [36, 37]. For the double racetrack spectrum in Fig. 3 b), the Vernier effect was observed in the normalized output spectrum. In this case, the circulation resonance from the microring interacts with the generated Fano resonance and induces a new spectrum that exhibits Vernier effect. The suppression that occurred in the resonance due to the Vernier effect made it possible to extend the FSR further [38]. The resonator also has a potential to be a highly sensitive device due the contribution of Vernier

effect [39]. Therefore, by optimizing the system which exhibits Fano resonance and with the additional presence of the Vernier effect, FSR and sensitivity can be enhanced significantly [16, 39]. Optical devices with high FSR are very desirable especially in the applications of the sensing field and as a building block for communication systems [40].

Fig. 4 a) shows the spectrum of optimized all-pass racetrack microring resonator with end-facet configuration, whereas Fig.4 b) shows the spectrum of optimized conventional all-pass racetrack configuration. Both systems were optimized to obtain the maximum FSR, and the parameters are shown in Table 2.

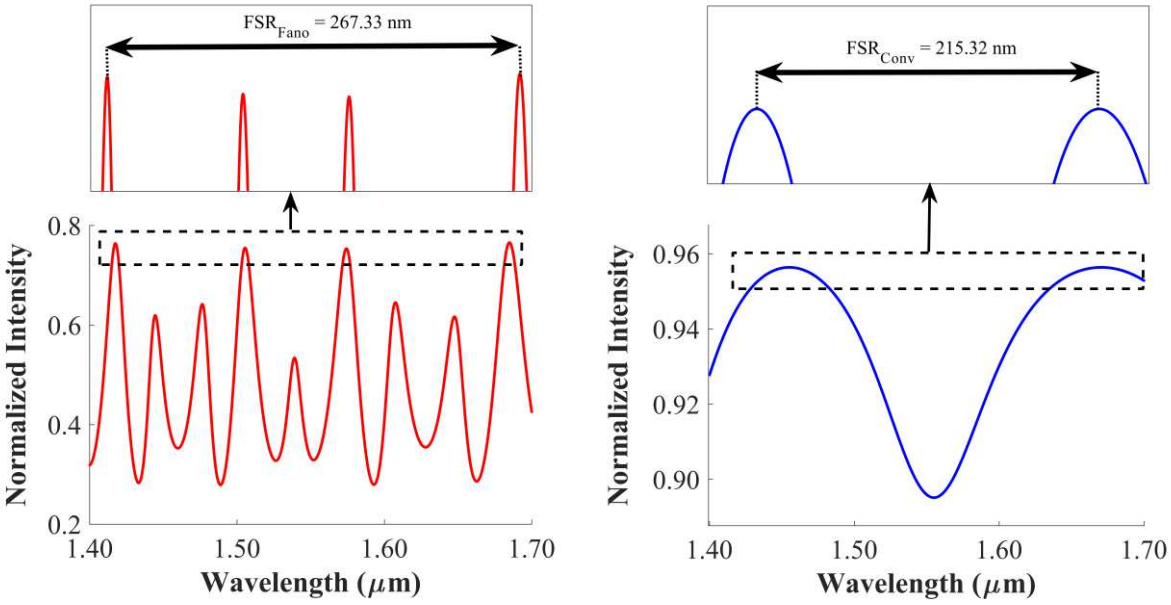


a) b)

**Fig. 4** a) The FSR of optimized racetrack microresonator with end-facet and b) the FSR of optimized conventional racetrack microresonator

The FSR for the optimized system with Fano resonance is 267.33 nm, while the FSR for the conventional system is 215.32 nm. There is a 19.45 % difference in FSR between the racetrack with Fano and the conventional racetrack system. Such a huge gap between the two systems brings significant outcome. Fig. 5 a) and b) show the spectrums for double racetrack microring resonator, in which one is a configuration with Fano while the other is the conventional configuration, respectively. Both configurations were optimized to obtain the maximum FSR. The optimized parameters are the radius of racetrack 1 and 2, and the length of waveguide for

the conventional waveguide. Meanwhile, for the configuration with Fano, the optimized parameter is the distance between end-facets. The optimized parameters are shown in Table 2.

Table 2: Optimized parameters for maximum FSR of the all-pass and double racetracks with Fano resonance and conventional configurations.

| Parameter | Racetrack | |
|---|---|---|
| | With Fano Resonance | Conventional |
| Radius | 15.263 µm | 4.00 µm |
| Length of waveguide | 30.000 µm | 30.00 µm |
| Coupling Coefficient | 0.95 | 0.95 |
| End-Facet Distance | 4.9474 µm | - |
| Parameter | Double Racetrack | |
| | With Fano Resonance | Conventional |
| Ring 1 Radius | 4.6897 µm | 2.00 µm |
| Ring 2 Radius | 6.5172 µm | 3.68 µm |
| Length of waveguide | 11.0 µm | 11.0 µm |
| Coupling Coefficient 1 | 0.95 | 0.95 |
| Coupling Coefficient 2 | 0.95 | 0.95 |
| End-Facet Distance | 10.5179 µm | - |

The FSR for the double racetrack with Fano resonance and the conventional double racetrack is 293.03 and 248.94 nm, respectively. The difference between two FSRs is 15.05%. The spectrums of both configurations with end-facet have larger FSR due to the suppression of interstitial peaks by Fano resonance [38]. Based on both optimizations, the presence of end-facet induces the suppression from Vernier effect and greatly improves the FSR. Besides, by comparing the all-pass racetrack with double racetrack configurations, the double racetrack microring has higher FSR compared to the all-pass racetrack.

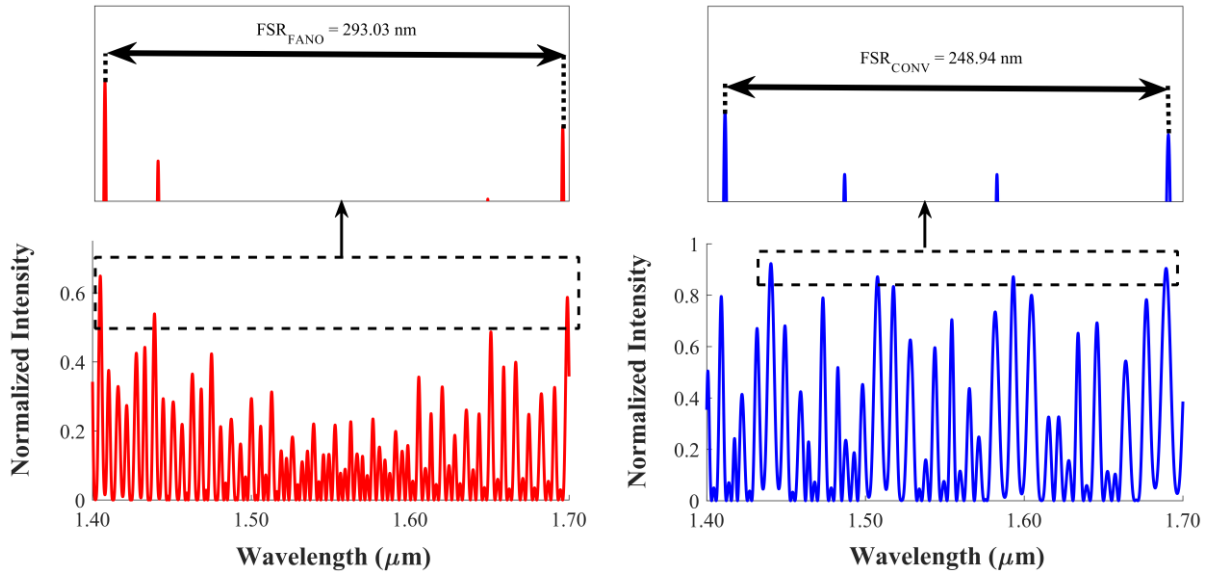


a) b)

**Fig. 5** a) The FSR of optimized double racetrack microresonator with end-facet and b) the FSR of optimized conventional double racetrack microresonator

In the following investigation, the coupling coefficient for all-pass racetrack microring and double racetrack was varied, and the behavior of the spectrum was analyzed. For the all-pass racetrack microring, the coupling coefficient was varied with three distinct values: 0.009, 0.09, and 0.9.

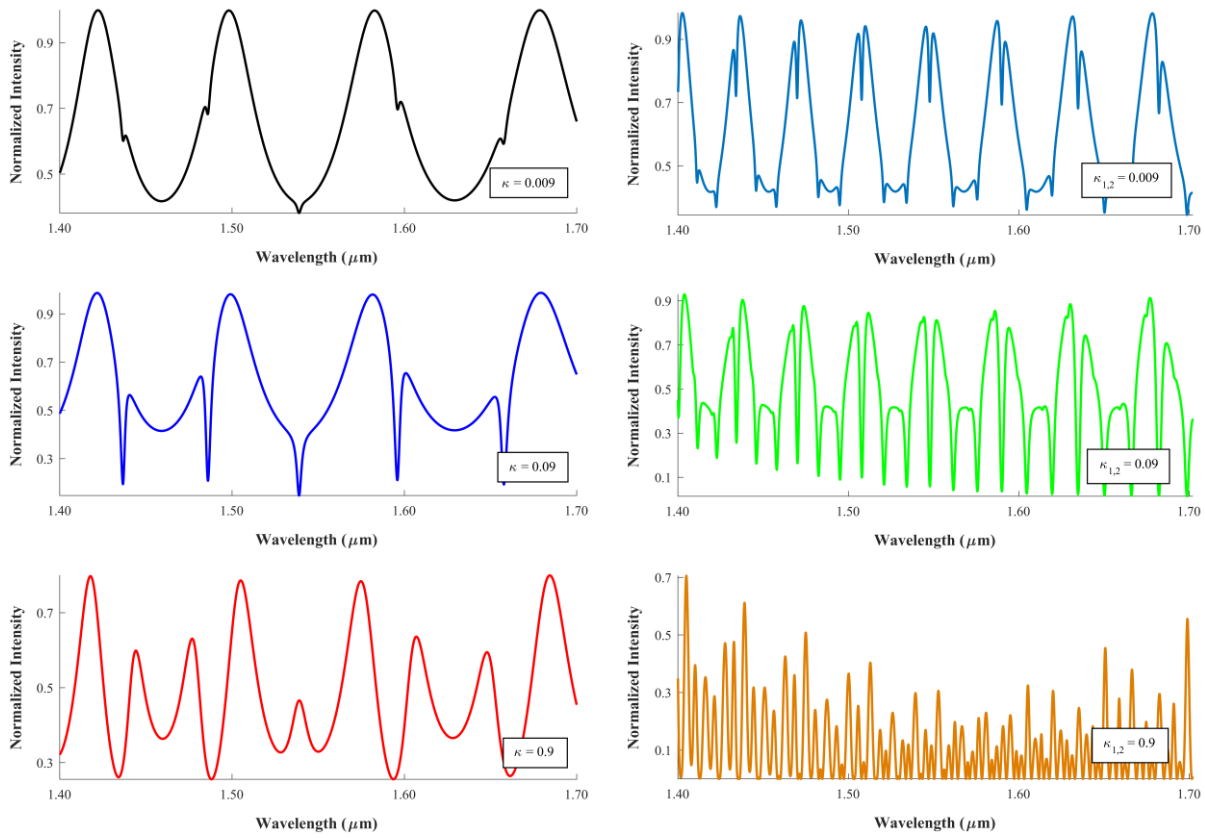


**Fig. 6** a) The spectrum for racetrack microring with Fano resonance. b) The spectrum for double racetrack microring with Fano resonance. Both spectrums were simulated using the previously optimized configurations which have maximum FSR

As shown in Fig. 6 a), as the coupling coefficient increased, the Fano resonance became more apparent. The measured FSR for $\kappa$ value of 0.009, 0.09, and 0.9 was 85.441, 85.821 and 266.58 nm, respectively. With the presence of Fano resonance, the circulation resonance is suppressed and the FSR of the spectrum can be extended significantly. However, the intensity of the light slightly decreased as the coupling coefficient increased. When $\kappa$ = 0.009, the maximum intensity was 0.998 whereas when $\kappa$ = 0.9, the maximum intensity decreased to 0.7996. The intensity loss was 19.88%. Fig. 6 b) shows the spectrum for double racetrack when the coupling coefficients, $\kappa_1$ and $\kappa_2$ of each racetrack were varied in pair for 0.009, 0.09, and 0.9 for each step. When $\kappa_1$ and $\kappa_2$ were set to 0.009, the spectrum behaved in way that there are successive of twin peaks. The FSR measured was 33 nm. As the coupling coefficient increased to 0.09, the Fano resonance line-shape became more obvious and from the spectrum, a small

suppression of the circulation resonance from 1.438 to 1.630 μm was observed. The FSR measured for $\kappa_{1,2}$ = 0.09 was 39 nm. As both coupling coefficients increased to 0.9, the suppression by Fano resonance increased significantly. The peaks on both left and right sides became more noticeable. Concurrently, the numerous peaks in the middle is suppressed, thus, improving the accuracy in measuring FSR. The measured FSR was 294 nm. There was a significant increment in FSR which has been extended due to the suppression by Fano resonance. In contrast with the all-pass racetrack microring system, the intensity of the double racetrack system decreased significantly when the coupling coefficients increased. When $\kappa_{1,2}$ = 0.009, the maximum intensity was 0.9833 while when $\kappa_{1,2}$ = 0.9, the maximum intensity was 0.754, showing an intensity loss of 28.23 %. These losses are quite large and not preferable. From the analysis, we can infer that by increasing the value of coupling coefficients, the FSR of the spectrum can be increased further and the visibility of the highest peak becomes clearer and more noticeable, thus making measurement involving highest peak easier. However, this benefit comes with a drawback: the output intensity will decrease. The decrement in intensity depends on the system used, the all-pass racetrack system only experienced 19.88 % loss, but the double racetrack system had a loss 28.23 %.

The sensitivity of both microrings was calculated through the wavelength shift technique. The sensitivity can be defined as

$$S = \frac{\Delta\lambda}{\Delta n} \text{ [7]}, \tag{8}$$

where $\Delta\lambda$ is shifted wavelength and $\Delta n$ is change in refractive index. High sensitivity device means that a slight variation in refractive index detected by the device, produces a large wavelength shift. The refractive index was varied by 0.001, 0.003, and 0.005 and the shifted wavelength was observed and measured. As shown in Fig. 7, the shifted wavelength of double racetrack system was noticeably larger compared to that of the all-pass racetrack system.

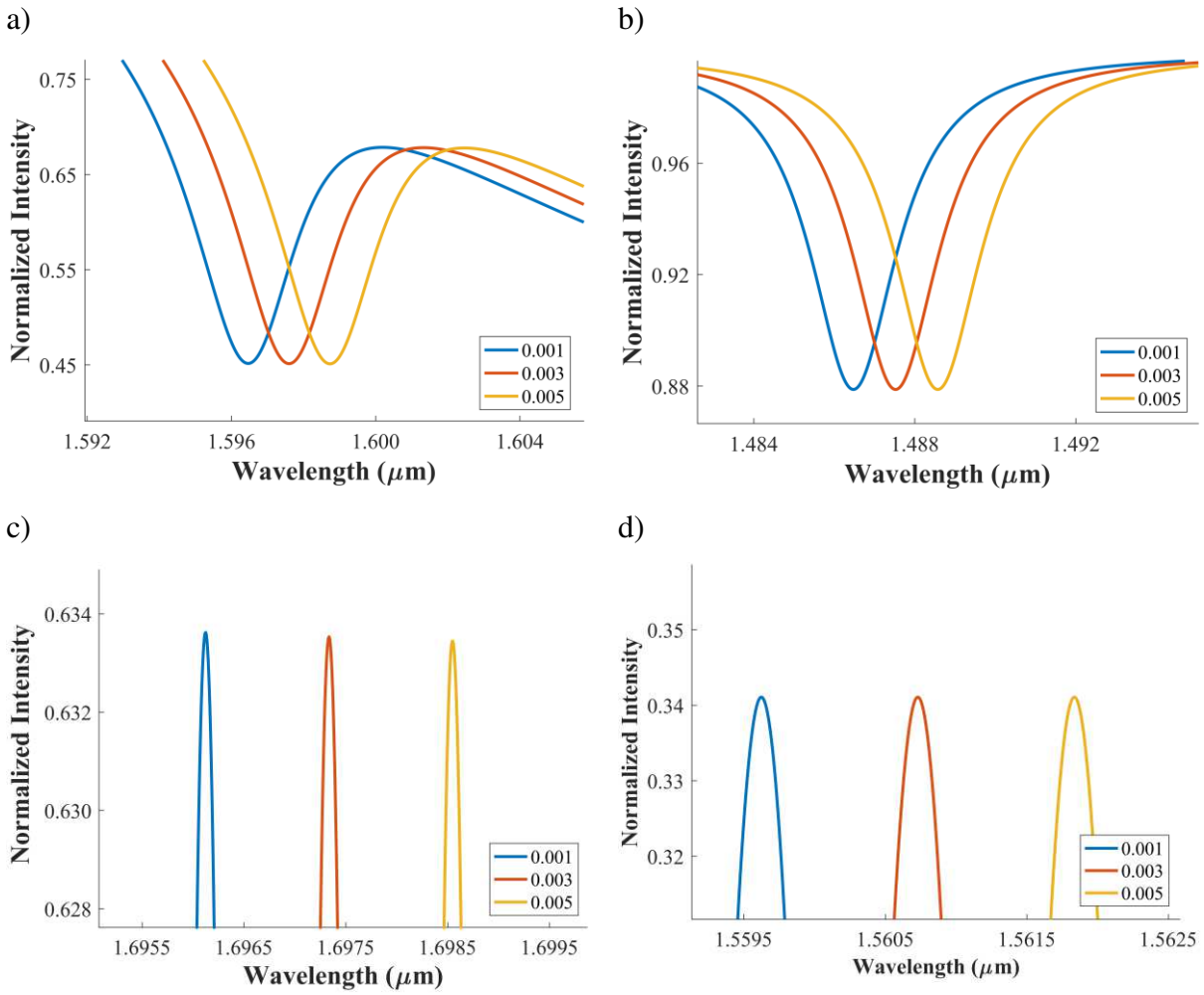


**Fig. 7** Wavelength shift of a) all-pass racetrack microring resonator with Fano resonance, b) conventional all-pass racetrack microring resonator, c) double racetrack microring resonator with Fano resonance, and d) conventional double racetrack

This phenomenon happens because the double racetrack has a longer length compared to the all-pass racetrack configuration. The resonance exposed to the change of refractive index is higher for the double racetrack, thus increasing the sensitivity. To compute the sensitivity of both systems, the change of refractive index was plotted against the shifted wavelength. Fig. 8 shows the sensitivity comparison between the all-pass racetrack microring and double racetrack microring with and without Fano resonance applied.

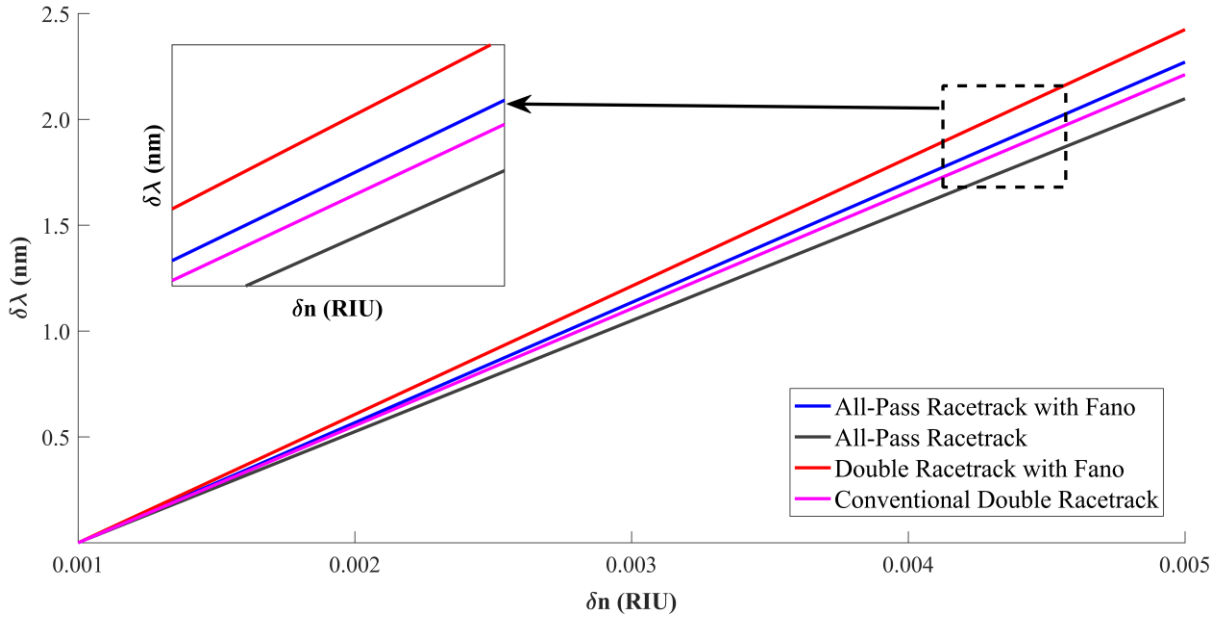


**Fig. 8** The sensitivity of all-pass and double racetrack microring with and without Fano resonance

The line with the steepest gradient shows the highest sensitivity. From Fig. 8, the double racetrack with Fano resonance is the most sensitive, followed by the all-pass racetrack as second, the double racetrack without Fano resonance and the all-pass racetrack microring without Fano resonance. The combination of double racetrack with end facet clearly indicates that Fano resonance can greatly enhance sensitivity. Table 3 shows the sensitivity for all configurations.

Table 3. Sensitivity and limit of detection for all configurations

| Configuration | Type of Resonance | Sensitivity (nm/RIU) | LOD (RIU/nm) |
|---|---|---|---|
| Double racetrack with Vernier and Fano resonance | Vernier Fano WGM | 606.00 | $3.30 \times 10^{-5}$ |
| All-Pass with Fano resonance | Vernier WGM | 567.75 | $3.52 \times 10^{-5}$ |
| Conventional double racetrack | Fano WGM | 552.80 | $3.62 \times 10^{-5}$ |
| Conventional all-pass | WGM | 524.25 | $3.81 \times 10^{-5}$ |

Table 3 shows that the double racetrack with end facet is the most sensitive. The sensitivity of all-pass racetrack configuration with end facet applied was compared with that of the conventional all-pass racetrack configuration. The all-pass racetrack with end facet applied was 5.16% more sensitive compared to the conventional all-pass racetrack configuration. The optimized double racetrack with end facet applied had a higher sensitivity by 6.31% compared to the conventional double racetrack microring. The LOD for each configuration was evaluated and listed in Table 3. The LOD is an important characteristic in sensing because it indicates the smallest scale that the configuration can measure, and, in this study, the double racetrack with Vernier and Fano resonance is the best configuration. There is a trend where, as sensitivity decreases, the LOD increases. From this, it can be inferred that LOD is inversely proportional with sensitivity.

This is expected due to two main factors: contact surface area and type of resonances. The double racetrack has more surface area that interacts with the change of the cladding's refractive index. This leads to the increment of the propagated light phase shift. Besides, the involvement of more resonance types enhances the sensitivity, in which the combination of the phase shift for every resonance type will affect the output spectrum. Comparatively between the two, the double racetrack with end facet is exceptionally sensitive to variations in refractive index, which makes it better choice to be implemented in optical sensing devices [41]. Through Fano resonance, ultrasensitive sensors can be achieved [42]. Therefore, integrating the Fano resonance into microring can enhance the sensitivity of an optical device.

## 4.0 CONCLUSION

In conclusion, the Fano-like resonance was generated by applying end facet reflection for all-pass racetrack and double racetrack microring resonator in the bus waveguide. The parameters such as the radius of ring, the distance between end facet, and the coupling coefficients were varied for both configurations. All the parameters' impacts on the output spectrum were analyzed, and the Vernier effect generated by the presence of Fano resonance were investigated, in order to optimize the FSR. The study explains the effect of various coupling coefficient values toward the Fano resonance, including the analysis of the resonance peak and intensity of the transmission. Both configurations with end facet obtained higher sensitivity than the conventional microring resonator configuration. By integrating Fano resonance, the overall performance of the resonator, including sensitivity and LOD, can be enhanced compared to the conventional configurations. This work is expected to be a good reference for improving and enhancing the sensitivity of all-optical devices.

**Acknowledgement**

This work was supported by CAPTOR and the Department of Physics, International Islamic University Malaysia, in term of facilities and financially by the Ministry of Education (Malaysia) through Fundamental Research Grant Scheme (Project No.: FRGS 19-033-0641) (References No.: FRGS/1/2018/TK07/UIAM/02/1).

**Disclosure**

The author declares no conflict of interest

## References


1. Hammer, M.: HCMT models of optical microring-resonator circuits. JOSA B. 27, 2237–2246 (2010)
2. Chao, C.Y., Guo, L.J.: Design and optimization of microring resonators in biochemical sensing applications. Journal of Lightwave Technology. 24, 1395–1402 (2006). https://doi.org/10.1109/JLT.2005.863333
3. Javanshir, S., Pourziad, A., Nikmehr, S.: Optical temperature sensor with micro ring resonator and graphene to reach high sensitivity. Optik. 180, 442–446 (2019). https://doi.org/https://doi.org/10.1016/j.ijleo.2018.11.124
4. He, Y., Ma, Y., Tong, Y., Yu, X., Peng, Z., Gao, J., Tittel, F.K.: Long distance, distributed gas sensing based on micro-nano fiber evanescent wave quartz-enhanced photoacoustic spectroscopy. Applied Physics Letters. 111, 241102 (2017). https://doi.org/10.1063/1.5003121
5. Sanati, P., Shafiee, A., Bahadoran, M., Akbari, E.: Label-free biosensor array comprised of Vernier microring resonator and 3× 3 optical coupler. The European Physical Journal Plus. 135, 1–14 (2020)
6. Campanella, C.E., Campanella, C.M., de Leonardis, F., Passaro, V.M.N.: A high efficiency label-free photonic biosensor based on vertically stacked ring resonators. The European Physical Journal Special Topics. 223, 2009–2021 (2014)
7. Ajad, A.K., Islam, M.J., Kaysir, M.R., Atai, J.: Highly sensitive bio sensor based on WGM ring resonator for hemoglobin detection in blood samples. Optik. 226, 166009 (2021)
8. Jiang, X., Jha, A.: Engineering of a Ge–Te–Se glass fibre evanescent wave spectroscopic (FEWS) mid-IR chemical sensor for the analysis of food and pharmaceutical products. Sensors and Actuators B: Chemical. 206, 159–169 (2015)
9. Jali, M.H., Rahim, H.R.A., Ashadi, M.J.M., Thokchom, S., Harun, S.W.: Applied microfiber evanescent wave on ZnO nanorods coated glass surface towards temperature sensing. Sensors and Actuators A: Physical. 277, 103–111 (2018)
10. Tian, C., Zhang, H., Li, W., Huang, X., Liu, J., Huang, A., Xiao, Z.: Temperature sensor of high-sensitivity based on nested ring resonator by Vernier effect. Optik. 204, 164118 (2020)
11. Seyfari, A.K., Bahadoran, M., Aghili, A.: Ultra-sensitive pressure sensor using double stage racetrack silicon micro resonator. Optical and Quantum Electronics. 52, 1–16 (2020)

12. Biswas, U., Rakshit, J.K., Bharti, G.K.: Design of photonic crystal microring resonator based all-optical refractive-index sensor for analyzing different milk constituents. Optical and quantum electronics. 52, 1–15 (2020)

13. Zheng, Y., Pu, M., Sahoo, H.K., Semenova, E., Yvind, K.: High-quality-factor AlGaAs-on-sapphire microring resonators. Journal of Lightwave Technology. 37, 868–874 (2019)

14. Zhao, G., Zhao, T., Xiao, H., Liu, Z., Liu, G., Yang, J., Ren, Z., Bai, J., Tian, Y.: Tunable Fano resonances based on microring resonator with feedback coupled waveguide. Optics express. 24, 20187–20195 (2016)

15. Yi, H., Citrin, D.S., Zhou, Z.: Highly sensitive silicon microring sensor with sharp asymmetrical resonance. Optics Express. 18, 2967–2972 (2010)

16. Boeck, R., Jaeger, N.A.F., Rouger, N., Chrostowski, L.: Series-coupled silicon racetrack resonators and the Vernier effect: theory and measurement. Optics express. 18, 25151–25157 (2010)

17. Troia, B., de Leonardis, F., Passaro, V.M.N.: Cascaded ring resonator and Mach-Zehnder interferometer with a Sagnac loop for Vernier-effect refractive index sensing. Sensors and Actuators B: Chemical. 240, 76–89 (2017)

18. Xu, Z., Sun, Q., Li, B., Luo, Y., Lu, W., Liu, D., Shum, P.P., Zhang, L.: Highly sensitive refractive index sensor based on cascaded microfiber knots with Vernier effect. Optics express. 23, 6662–6672 (2015)

19. Gu, L., Fang, H., Li, J., Fang, L., Chua, S.J., Zhao, J., Gan, X.: A compact structure for realizing Lorentzian, Fano, and electromagnetically induced transparency resonance lineshapes in a microring resonator. Nanophotonics. 8, 841–848 (2019)

20. He, Z., Xue, W., Cui, W., Li, C., Li, Z., Pu, L., Feng, J., Xiao, X., Wang, X.: Tunable Fano resonance and enhanced sensing in a simple Au/TiO2 hybrid metasurface. Nanomaterials. 10, 687 (2020)

21. Vollmer, F., Schwefel, H.G.L.: Taking detection to the limit with optical microcavities: Recent advances presented at the 560. WE Heraeus Seminar, (2014)

22. Azuelos, P., Girault, P., Lorrain, N., Poffo, L., Hardy, I., Guendouz, M., Thual, M.: Theoretical investigation of Vernier effect based sensors with hybrid porous silicon-polymer optical waveguides. Journal of Applied Physics. 121, 144501 (2017)

23. Han, Z., Xin, G., Nan, P., Liu, J., Zhu, J., Yang, H.: Hypersensitive high-temperature gas pressure sensor with Vernier effect by two parallel Fabry-Perot interferometers. Optik. 241, 166956 (2021)

24. Liu, Y., Li, X., Zhang, Y., Zhao, Y.: Fiber-optic sensors based on Vernier effect. Measurement. 167, 108451 (2021)

25. Troia, B., Khokhar, A.Z., Nedeljkovic, M., Penades, J.S., Passaro, V.M.N., Mashanovich, G.Z.: Cascade-coupled racetrack resonators based on the Vernier effect in the mid-infrared. Optics express. 22, 23990–24003 (2014)

26. Wang, F., Wang, X., Zhou, H., Zhou, Q., Hao, Y., Jiang, X., Wang, M., Yang, J.: Fano-resonance-based Mach-Zehnder optical switch employing dual-bus coupled ring resonator as two-beam interferometer. Optics express. 17, 7708–7716 (2009)

27. Zheng, S., Ruan, Z., Gao, S., Long, Y., Li, S., He, M., Zhou, N., Du, J., Shen, L., Cai, X.: Demonstration of on-chip tunable Fano resonance based on interference between microring resonator and Fabry-Perot cavity. In: 2017 Asia Communications and Photonics Conference (ACP). pp. 1–3. IEEE (2017)

28. Noorden, A.F.A., Mohamad, A., Salleh, M.H., Daud, S., Mohamad, S.N., Ali, J.: Free spectral range analysis of double series microresonator system for all-optical corrosion sensor. Optical Engineering. 59, 17106 (2020)

29. Fan, S.: Sharp asymmetric line shapes in side-coupled waveguide-cavity systems. Applied Physics Letters. 80, 908–910 (2002)

30. Ariannejad, M.M., Akbari, E., Thong, P.Y., Ghasemi, M., Dehzangi, A., Ahmad, H.: Silicon racetrack resonator based on nonlinear material. The European Physical Journal D. 73, 1–5 (2019)

31. Larre, P.-E., Biasi, S., Ramiro-Manzano, F., Pavesi, L., Carusotto, I.: Pump-and-probe optical transmission phase shift as a quantitative probe of the Bogoliubov dispersion relation in a nonlinear channel waveguide. The European Physical Journal D. 71, 1–17 (2017)

32. Heebner, J., Grover, R., Ibrahim, T.: Optical microresonator theory. Springer (2008)

33. Fan, H., Fan, L., Xia, C., Wang, L., Shen, M.: Tunable Fano-like resonance analysis based on a system consisting of a two-silica-microdisk-coupled Mach–Zehnder interferometer and graphene. JOSA B. 34, 2429–2435 (2017)

34. Chauhan, D., Adhikari, R., Saini, R.K., Chang, S.H., Dwivedi, R.P.: Subwavelength plasmonic liquid sensor using Fano resonance in a ring resonator structure. Optik. 223, 165545 (2020)

35. Hu, F., Chen, F., Zhang, H., Sun, L., Yu, C.: Sensor based on multiple Fano resonances in MIM waveguide resonator system with silver nanorod-defect. Optik. 229, 166237 (2021)

36. Ngo, Q.M., Le, K.Q., Vu, D.L.: Optical bistability based on Fano resonances in single- and double-layer nonlinear slab waveguide gratings. JOSA B. 31, 1054–1061 (2014)

37. Nguyen, T.K., Le, T.D., Dang, P.T., Le, K.Q.: Asymmetrically engineered metallic nanodisk clusters for plasmonic Fano resonance generation. JOSA B. 34, 668–672 (2017)

38. Boeck, R., Jaeger, N.A.F., Chrostowski, L.: Experimental demonstration of the Vernier effect using series-coupled racetrack resonators. In: 2010 International Conference on Optical MEMS and Nanophotonics. pp. 1–2. IEEE (2010)

39. Zhao, Y., Wang, P., Lv, R., Liu, X.: Highly sensitive airflow sensor based on Fabry–Perot interferometer and Vernier effect. Journal of Lightwave Technology. 34, 5351–5356 (2016)

40. Fegadolli, W.S., Vargas, G., Wang, X., Valini, F., Barea, L.A.M., Oliveira, J.E.B., Frateschi, N., Scherer, A., Almeida, V.R., Panepucci, R.R.: Reconfigurable silicon thermo-optical ring resonator switch based on Vernier effect control. Optics express. 20, 14722–14733 (2012)

41. Fang, L., Gu, L., Zheng, J., Zhao, Q., Gan, X., Zhao, J.: Controlling resonance lineshapes of a side-coupled waveguide-microring resonator. Journal of Lightwave Technology. 38, 4429–4434 (2020)

42. Li, W., Zhang, H., Liu, J., Lin, J., Xue, X., Zhang, X., Xu, X., Huang, A., Xiao, Z.: On-chip high-sensitivity temperature sensor based on gain–loss coupled microresonators. JOSA B. 34, 1765–1770 (2017)